A Particle Finite Element-Based Framework for Differentiation Paths of Stem Cells to Myocytes and Adipocytes

Hybrid Cell-Based and Finite Element Modeling

Vermolen, F. J.; Harrevelt, Seb; Gefen, A.; Weihs, D.

DOI
10.1016/B978-0-12-811718-7.00009-5

Publication date
2018

Document Version
Final published version

Published in
Numerical Methods and Advanced Simulation in Biomechanics and Biological Processes

Citation (APA)
Vermolen, F. J., Harrevelt, S., Gefen, A., & Weihs, D. (2018). A Particle Finite Element-Based Framework for Differentiation Paths of Stem Cells to Myocytes and Adipocytes: Hybrid Cell-Based and Finite Element Modeling. In M. Cerrolaza, S. Shefelbine, & D. Garzón-Alvarado (Eds.), *Numerical Methods and Advanced Simulation in Biomechanics and Biological Processes* (pp. 171-185). Elsevier. https://doi.org/10.1016/B978-0-12-811718-7.00009-5

Important note
To cite this publication, please use the final published version (if applicable).
Please check the document version above.

Chapter 9

A Particle Finite Element–Based Framework for Differentiation Paths of Stem Cells to Myocytes and Adipocytes: Hybrid Cell–Based and Finite Element Modeling

F.J. Vermolen[1], S.D. Harrevelt[1], A. Gefen[2] and D. Weihs[3]

[1]*Delft University of Technology, Delft, The Netherlands;* [2]*Tel Aviv University, Tel Aviv, Israel;* [3]*Technion–Israel Institute of Technology, Haifa, Israel*

9.1 INTRODUCTION

Differentiation of mesenchymal stem cells is an important (sub)process in many biological and medical phenomena related to tissue maintenance, regeneration, healing, and tissue repair, or to development of pathologies such as cancer and tissue atrophies. See Wu et al. (2007) for a study where cell differentiation of mesenchymal stem cells enhances wound healing. To prevent or treat certain diseases, or to enhance the health of individuals, various treatment procedures aim at revising the differentiation paths of (stem) cells, see Sell (2004) and Yan and Liu (2016) for applications in the framework of cancer. Because cell differentiation merely represents a specialization of cells to perform a certain biological task, the differentiation process of a cell depends largely not only on its environment but also on genetic programming and also age or a disease, when relevant. See for instance Guilak et al. (2010) for a presentation of stem cell fate by interactions with its environment and Stolzing et al. (2007) for more information about the influence of age on the differentiation of bone marrow–derived mesenchymal stem cells. It is well known that stimuli for cell differentiation that originate from the environment (locally or globally) can have varying natures, such as mechanical or chemical. A common treatment of patients involving stem cells, primarily in the field called regenerative medicine, is therefore aimed at influencing the differentiation pathways by modifying the mechanics and/or biochemical nature of the cell environment, see Gimble et al. (2007) for instance.

Considering biomedical processes such as wound healing, contractures as a result of large damage, formation of hypertrophic scars, initiation, and progression of cancer have been modeled in various studies. One may distinguish between various kinds of mathematical models on different scales, such as tissue scale, or cell colony-scale or even (sub)cellular scales. In this work, we will limit ourselves to the cell colony scale, where individual cells are considered in interaction with their environment through which they migrate and where they change their phenotypes. Some of the early cell-scale models have been developed by Drasdo and Höhme (2005) and Groh and Louis (2010). The experimental work by Reinhart-King et al. (2008) indicated that cells on a substrate communicate with each other through mechanical pulling forces that are exerted on the substrate if the forces exceed a certain threshold. Based on this observation, later different colony-scale models were constructed by Rey and Garcia-Aznar (2013) and Mousavi et al. (2013). Bookholt et al. (2016), Vermolen et al. (2015), Vermolen and Gefen (2015) and Vermolen (2015) extended the models to applications in contraction in burns and to model the early stages of cancer. The work of Bookholt et al. (2016) is, as far as we know, the

Numerical Methods and Advanced Simulation in Biomechanics and Biological Processes. https://doi.org/10.1016/B978-0-12-811718-7.00009-5

first to apply the cell-based formalism to modeling angiogenesis. Angiogenesis was classically modeled by cellular automata or in particular cellular Potts models for example by Van Oers et al. (2014), where cell differentiation was only addressed in few of those works. Vermolen and Gefen (2015) model cell differentiation from fibroblasts to myofibroblast through entirely stochastic principles, where it is assumed that the probability of cell differentiation satisfies an exponential distribution, which is a special case of a Poisson process.

Differentiation phenomena have been modeled in biological context using different approaches. Most of the classical models treat cells at a continuum scale, in terms of population densities, cells per unit of volume (or area), using partial differential equations (PDEs). These PDEs generally contain terms for, if applicable, cell migration (by random walk, chemotaxis, haptotaxis, or tensotaxis), cell proliferation and death, and cell differentiation. In most classical models, cell differentiation is modeled by the inclusion of a reaction-like term, implying immediate, yet in many cases, incomplete differentiation. Recently, Prokharau et al. (2012, 2014) formulated a mathematical framework where the differentiation of each cell takes place over nonzero, finite intervals of time. The model is based on solving PDEs with a specified maturation space parameter. In that formalism, cells are hypothesized to achieve only one phenotype (fate) to minimize the dimensionality of the maturation space. The stem cells are then divided into several "groups" representing the various phenotypes that the stem cells may differentiate to.

In this chapter, we modify the formalism of Prokharau et al. (2012, 2014) where we treat the cells as discrete objects, that is, we take a cell-based modeling approach. The formalism to be developed is, as far as we know, original. We will illustrate potential applications of the model to differentiation processes that are relevant to tissue disuse, e.g., after a spinal cord injury (see Fig. 9.1 for an illustration); similar effects may occur with aging or with a sedentary lifestyle. First, we present the mathematical framework for the differentiation of mesenchymal stem cells to two different phenotypes and, subsequently, we extend the framework to a generic number of phenotypes a cell can differentiate to. Then, we show computations that illustrate the formation of skeletal muscle and fat tissues and the muscle/fat tissue balance. Finally, we will discuss the current framework. We note that the chapter has been written to meet the scope of the book, which is being descriptive in the numerical methodology, rather than digressing about the model results and implications. The present model falls within the class of hybrid models, where cells are treated as identities, and concentration as well as mechanical quantities are treated as field parameters that follow from the solving PDEs. Summarized, the key points of the current chapter are the following:

- We describe a hybrid method on cellular scale where cells are treated as individual objects and where the solution of PDEs (concentrations and mechanical balance) is approximated by the finite element method.
- The formalism is applied to cell differentiation where stem cells interacting with muscle and fat cells are considered.
- The numerical method contains both deterministic and stochastic processes.

Furthermore, we only provide the most important references that were used in this study in the present chapter. If the reader is interested in a more in-depth explanation on various modeling approaches, including full continuum-scale models, we refer to our reviews in Weihs et al. (2016) and Vermolen (2015).

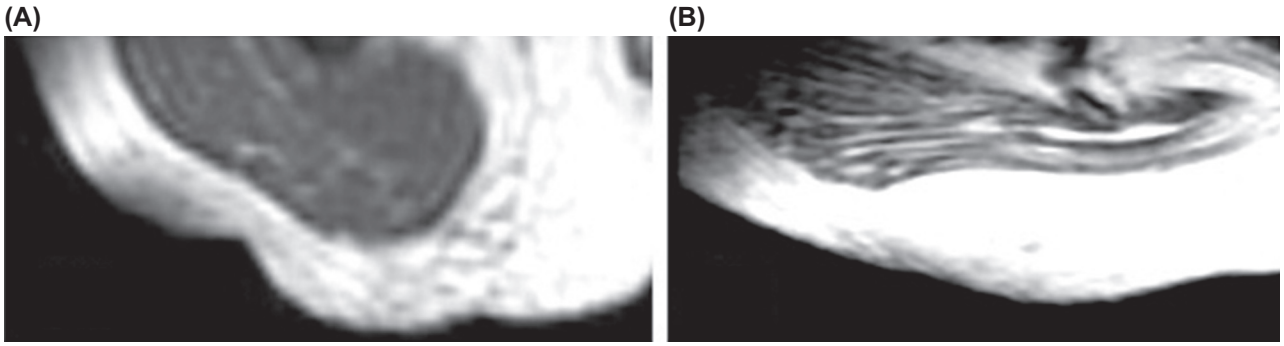

FIGURE 9.1 The influence of disuse on muscle/fat contents in humans can be demonstrated by means of magnetic resonance imaging: (A) healthy gluteus muscle (dark) and surrounding subcutaneous fat tissue in the buttocks (white). A relatively small, normal mass of intramuscular adipose tissue can be observed within the muscle tissue. (B) Gluteus muscle (dark) showing severe fat infiltration (white straps) intramuscularly, and an increased thickness of subcutaneous fat at the same anatomical site, in an individual within a year after a spinal cord injury (SCI). The intramuscular fat in both individuals contains mesenchymal stem cells, but apparently, the differentiation fate of these cells was biased toward the adipocyte phenotype in the SCI case, where the mechanical stimuli influencing stem cell differentiation where altered to the static regime due to the disuse.

9.2 THE MATHEMATICAL FRAMEWORK

First, we present the model as we apply it to the differentiation of mesenchymal stem cells to two different phenotypes and, subsequently, we show its extension to any number of phenotypes.

9.2.1 A Ternary Cell System

We illustrate the effect of use (e.g., physical exercise) or disuse (e.g., a sedentary lifestyle) on the composition of the tissue by considering stem cells that have the ability to differentiate to either myocytes or adipocytes; those are, respectively, muscle and fat cells. The myocytes are cells that gradually acquire the ability to contract, being the contractile components of skeletal muscles. The adipocytes are cells that build up triglyceride depots in the form of lipid droplets (LDs), used for storage of energy. These LDs increase in size during the differentiation to adipocytes, causing the adipocytes to grow substantially in volume as adipogenesis progresses in a process called hypertrophy. At the macroscopic scale, the outcome would be increased fat tissue mass, which can lead to obesity. The interested reader is referred to Shoham et al. (2014) and Gefen and Benayahu (2015). In a physiological environment, adipose-derived stem cells, myocytes, and adipocytes exist in adjacent populations. For example, skeletal muscles contain intramuscular fat (fat depots within the muscles) that provide readily available energy supply to muscles. The intramuscular fat in turn contains mesenchymal stem cells that are potentially able to either build or repair the surrounding muscle tissue mass. The tissue is supplemented by mesenchymal stem cell differentiation into myoblasts and further into myocytes, or, alternatively, these cells are able to gradually differentiate into adipocytes, which will eventually increase the fat tissue mass, intramuscularly or extramuscularly. Differentiation pathways of adipose-derived stem cells (into either myocytes or adipocytes) are determined by genetics, age, and presence of a disease and, importantly, by the influence of the environment, including the mechanical and chemical environment, and by biomolecular signaling from surrounding cells.

9.2.1.1 Differentiation Model

The modeling presented here takes into account that stem cells gradually acquire the phenotype they are differentiating to. The mathematical formalism for the differentiation process is based on the following assumptions:

Assumption 1: Complete cell differentiation is irreversible: a stem cell that has *fully* differentiated to a certain phenotype, cannot dedifferentiate. That is, dedifferentiation is only possible if the differentiation process has not yet completed and the cell did not acquire the complete set of biological features of the phenotype.
Assumption 2: A stem cell is able to gradually adopt the properties of *only one* phenotype.

From the second assumption, it follows that if a cell's chemicomechanical environment dictates that it differentiates toward another phenotype, then it will first dedifferentiate and subsequently differentiate toward the other phenotype. These two assumptions were also used in the model of Prokharau et al. (2012, 2014), where both assumptions gave important implications on the boundary conditions in the *maturation* space (well posedness). Furthermore, Assumption 2 reduced the dimensionality of the maturation space in the model of Prokharau et al. (2012, 2014). As we model cells individually, let us consider a population of n_c (t) cells, where t denotes time and the number of cells may vary with time as a result of cell proliferation, cell death, or applied treatments (e.g., injection or local delivery of stem cells). Let $j \in \{1,\ldots, n_c\}$ be the index of a viable cell. For each cell, we introduce the maturation parameter $a_j \in [0, 1]$ such that it represents the extent by which a cell j has adopted the properties of a certain phenotype given by $e_j \in \{1, 2\}$. The functional behavior of a_j over time represents the evolutionary differentiation path of cell j. If $a_j \in (0, 1)$ then cell j is a stem cell (possibly attaining the properties of either phenotype), and if $a_j = 1$ then cell j has fully differentiated to either phenotype, whereas $a_j = 0$ represents the situation where cell j is still fully undifferentiated (that is, at the stem cell state). Further, $e_j = 1$ and $e_j = 2$, respectively, correspond to the phenotype myocyte and adipocyte.

Hence, at this stage, we consider the possibility that stem cells can differentiate to either myocytes or adipocytes and we use the following convention for the pair a_j and e_j; this is summarized in

$$(a_j(t), e_j(t)): \begin{cases} = (1,1), & \text{myocyte (M)}, \\ \in (0,1) \times \{1\}, & \text{tending to myocyte}, \\ = 0 \times \{1,2\}, & \text{undifferentiated stemcell (S)}, \\ \in (0,1) \times \{2\}, & \text{tending to adipocye}, \\ = (1,2), & \text{adipocyte (A)}. \end{cases} \tag{9.1}$$

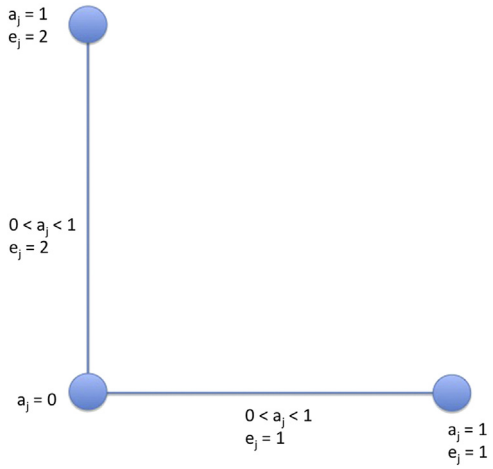

FIGURE 9.2 A schematic of the differentiation pathway that is represented via the $a-$parameter.

The situation is schematically depicted in Fig. 9.2. The adipocyte and myocyte phenotypes are represented by (A) and (M), respectively. Let $U = U\left(t, \mathbf{x}, \underline{\psi}, a\right)$ be the differentiation rate of cell j, which depends on time, spatial location $\mathbf{x}$, and p stimuli $\underline{\psi} = \left[\psi_1, \ldots, \psi_p\right]^T$; the gradual transition of stem cells is modeled by

$$\frac{da_j}{dt} = U\left(t, \mathbf{x}(t), \underline{\psi}(t), a_j(t)\right), \quad a_j(0) = a_j^0. \tag{9.2}$$

Here we also take into account the spatial migration ability of the cell. We assume that cells gradually lose their ability to migrate as they differentiate, so that a mesenchymal stem cell is fully mobile, but once it has started differentiating, say to a preadipocyte, this ability decreases and is completely lost when reaching full maturation. Indeed, mature adipocytes are not mobile, and neither are fully differentiated myocytes; therefore, for example, for muscle cells, the migration ability is lost in the transition from myoblasts to myocytes.

9.2.1.2 Chemical Signals

In this application, the differentiation rate depends on two chemical stimuli and on a mechanical stimulus. The chemical stimuli are signaling molecules (e.g., cytokines) that are secreted by already differentiated adipocytes and myocytes and to a lesser extent by stem cells that are in the process of adopting the properties of these phenotypes. This assumption is motivated by the observed adjustment of the cells to the behavior and phenotype of their nearest neighbors (see, for instance, Shoham et al., 2014; Or-Tzadikario et al., 2010). The distribution of the signaling molecules c_M and c_A over the domain Ω, bounded by $\partial\Omega$, that are released by myocytes and adipocytes, respectively, is, for $k \in \{M, A\}$, modeled by linear diffusion:

$$\begin{aligned}
&\frac{\partial c_k}{\partial t} + \nabla \cdot (\mathbf{v}_m c_k) - D_k \Delta c_k = \sum_{j=1}^{n_c(t)} \sum_{i=1}^{L} \gamma_k^i(a_j, e_j)\delta(\mathbf{x} - \mathbf{x}_j(t))\Delta A_j^i(t) + S_k(t, \mathbf{x}), \\
&c_k(0, \mathbf{x}) = 0, \quad \mathbf{x} \in \overline{\Omega}, \\
&D_k \frac{\partial c_k}{\partial \mathbf{n}} + \kappa c_k = 0, \quad \mathbf{x} \in \partial\Omega.
\end{aligned} \tag{9.3}$$

The second term on the left-hand side in the above equation represents passive convection as a result of the movement of the mesh over the domain, including the extracellular matrix and the cells. The mesh velocity is given by $\mathbf{v}_m$, and this velocity results from the displacements of the nodes caused by the time evolution of the forces that are applied by the cells. In other words, we have $\mathbf{v}_m = \frac{d}{dt}\mathbf{u}(t, \mathbf{x}(t))$, where the total (or material) derivate of the displacements is used. The third term on the left-hand side in the above PDE accounts for linear diffusion of the cytokine. The first term on the right-hand side contains the Dirac Delta function and accounts for the production of the cytokine by the individual cells depending on

their differentiation state. It involves a summation over all cells, as well as over the boundary segments of the cells. The second term in the right-hand side defines any other addition of the cytokine as a result of applied treatments and therapies. The boundary condition reflects the fact that the boundary of the domain cannot be taken infinitely far away and that the outflow on the boundary is balanced by the flow into the tissue away from the domain of computation. Both cytokine concentrations, released by either (pre)adipocytes or myoblasts, which are modeled as premyocytes, and myocytes, act as chemical stimuli for the differentiation path of the stem cells. The amount of cytokines that is injected by each stem cell depends on its maturation. In this study, we use a linear relationship where we normalize with respect to the total area of the cell boundary curve:

$$\gamma^{j}_{k}(a_j, e_j) = \frac{\gamma^{0}_{k}\, a_j}{\sum_{i=1}^{L} \Delta A^{i}_{j}}\, \delta_{k,e_j}, \tag{9.4}$$

where $\delta_{k,\,ej}$ represents the Kronecker Delta, j is the cell number, and the summation over indexes i is carried out over the boundary segments of cell j. We realize that any relationship can be used here as long as the amount of production increases for the particular phenotype as a moves away from zero. From the concentration of myokine or adipokine, the chemical stimulus is determined by the use of the average concentration that is experienced by the nodal points on the boundary of the cell. For cell i, this concentration is calculated by

$$c^{i}_{k}(t) = \frac{1}{L}\sum_{j=1}^{L} c_k\left(t, \mathbf{x}^{i}_{j}\right), \quad k \in \{M, A\}. \tag{9.5}$$

9.2.1.3 Differentiation Rate and Stimuli

Next, we treat the function for the differentiation rate. To this extent, we use

$$u = u\left(t, \mathbf{x}, \underline{\psi}, a\right) = \frac{1}{2}\left(u_c(\psi_1, \psi_2) + u_m(\psi_3)\right), \tag{9.6}$$

where u_c and u_m, respectively, represent the chemical and mechanical contributions to the stimulus. For the chemical stimulus, we set

$$\psi_1 = c_M, \quad \psi_2 = c_A. \tag{9.7}$$

We use the following assumption for the function u_c:
Assumption 3: Consider cell j, then

1. If $e_j = 1$ (cell j is acquiring myocyte properties), then

$$u_c: \begin{cases} < 0, & c_M < c_A, \\ = 0, & c_M = c_A, \\ > 0, & c_M > c_A; \end{cases}$$

2. If $e_j = 2$ (cell j is acquiring adipocyte properties), then

$$u_c: \begin{cases} < 0, & c_A < c_M, \\ = 0, & c_M = c_A, \\ > 0, & c_A > c_M; \end{cases}$$

Consider ψ_3, u_m (ψ_3), and let $\widetilde{\psi} \in \mathbb{R}$, then the mechanical stimulus is treated analogously, using the following assumption.

Assumption 4: Consider cell j, then

1. If $e_j = 1$ (cell j is acquiring myocyte properties), then

$$u_m: \begin{cases} < 0, & \psi_3 < \widetilde{\psi} \\ = 0, & \psi_3 = \widetilde{\psi}, \\ > 0, & \psi_3 > \widetilde{\psi}; \end{cases}$$

2. If $e_j = 2$ (cell j is acquiring adipocyte properties), then

$$u_m: \begin{cases} < 0, & \psi_3 > \widetilde{\psi} \\ = 0, & \psi_3 = \widetilde{\psi} \\ > 0, & \psi_3 < \widetilde{\psi}; \end{cases}$$

From these assumptions, the following proposition is proved:

Proposition 1: Let Assumptions 3 and 4 be valid, then

$$(-1)^{e_j-1} u_c \cdot (c_M - c_A) \geq 0, \quad \text{and } (-1)^{e_j-1} u_m \cdot \left(\psi_3 - \widetilde{\psi}\right) \geq 0. \tag{9.8}$$

Proof: We prove the first inequality on the left. Let $e_j = 1$, then, according to Assumption 3, $c_M < c_A$ implies $u_c < 0$, and hence $u_c\,(c_M - c_A) > 0$ and hence $(-1)^{e_j-1} u_c \cdot (c_M - c_A) > 0$. Further, if $c_M > c_A$, then from Assumption 3, we have $u_c > 0$ and hence again this yields $u_c\,(c_M - c_A) > 0$ and $(-1)^{e_j-1} u_c \cdot (c_M - c_A) > 0$. Case 2, where $e_j = 2$, is treated analogously. Further, $c_M = c_A$ implies $(-1)^{e_j-1} u_c \cdot (c_M - c_A) = 0$ directly. The second inequality is proved similarly. □

To have a chemical component for the maturation speed that satisfies the above assumption, we set

$$u_c(\psi_1, \psi_2; e_j) = \overline{u}(\psi_1 - \psi_2; e_j) = (-1)^{e_j-1}\, U_M \tanh\left(\frac{c_M - c_A}{\xi}\right) = (-1)^{e_j-1}\, U_M \tanh\left(\frac{\psi_1 - \psi_2}{\xi}\right), \tag{9.9}$$

where U_M, $\xi > 0$, respectively, represent the maximal differentiation speed and the slope of the transition between the two cell phenotypes. It is immediately clear that the above relation immediately satisfies the prerequisites of Proposition 1. The mechanical stimulus, ψ_3, is used analogously as follows:

$$u_m(\psi_3; e_j) = (-1)^{e_j-1}\, U_M \tanh\left(\frac{\psi_3 - \widetilde{\psi}}{\eta}\right), \quad U_M \geq 0, \tag{9.10}$$

where $\widetilde{\psi}$ and η, respectively, represent the point of transition that the mechanical stimulus changes its phenotypical direction and the slope of the transition between the two cell phenotypes. The octahedral shear strain (also known as the engineering shear strain on an octahedral plane, where the octahedral plane is a plane that is oriented equally with respect to the principal axes), ϕ, is computed from

$$\phi = \frac{1}{3}\sqrt{(\varepsilon_1 - \varepsilon_2)^2 + (\varepsilon_1 - \varepsilon_3)^2 + (\varepsilon_2 - \varepsilon_3)^2}, \tag{9.11}$$

where ε_l represent the principle strains (eigenvalues of the strain tensor). The mechanical stimulus is based on the history path of the octahedral shear strain a cell is exposed to. Because the variations in ϕ over time is of importance rather than the octahedral shear strain at a specific time instant, we use the following integral expression

$$\psi_3(t, \mathbf{x}_j(t)) = \int_{(t-\tau)_+}^{t} w(s)\left(\frac{d\phi}{ds}(s, \mathbf{x}_j(s))\right)^2 ds. \tag{9.12}$$

Here τ represents the length of the time interval that has an impact on the differentiation behavior at certain time t. The nonnegative function $w\,(s)$ has been added as a weight function to account for larger influences at the latest times before time t. We use the following kernel for $w\,(s)$:

$$w(s) = e^{s-t}. \tag{9.13}$$

Because we only want the transformation to muscle cells (myocytes) to occur if the cellularly experienced octahedral strain is subject to a sufficiently high frequency, we apply a high-pass filter on ϕ to suppress the influence of low frequency components.

9.2.1.4 The Cell Geometry and Its Evolution

The cells are modeled with evolving geometry where the myocytes are modeled as ellipses with a large eccentricity (aspect ratio), and in contrast the adipocytes are modeled as circles that expand as they mature. To this end, we describe the 2D case; the 3D case is treated analogously. The cell boundary is divided into nodal points $j \in \{1,\ldots, N\}$. Note that for the 2D case the number of nodal points is equal to the number of elements on the cell boundary. Let the axes of the elliptical geometry be given by $L(t)$ and $W(t)$, then we have for cell i

$$x_j^i(t) = L^i(t)\cos\left(\frac{2\pi j}{N}\right), \quad y_j^i(t) = W^i(t)\sin\left(\frac{2\pi j}{N}\right). \tag{9.14}$$

From this relation, it is clear that the outward unit normal vector is given by

$$\mathbf{n}_j^i(t) = \left[\frac{x_j^i(t)}{L^i(t)}, \frac{y_j^i(t)}{W^i(t)}\right]^T. \tag{9.15}$$

Because the cell is allowed to migrate to different directions, its orientation changes over time, and to this extent, rotation of the cell is incorporated by the rotation matrix given by

$$R(\theta_i) = \begin{pmatrix} \cos(\theta_i) & -\sin(\theta_i) \\ \sin(\theta_i) & \cos(\theta_i) \end{pmatrix}, \tag{9.16}$$

where θ_i is the angle of cell i with respect to the x-axis. The above rotation matrix is applied via left multiplication by the coordinates of the cell boundary. Note that in the present model only elliptic cell shapes are allowed. The normal vector will be used for the determination of the force vector on each boundary segment. Next we consider the geometrical evolution of the cells. We assume that the cell dimensions are entirely determined by the degree of maturation and the phenotype they are differentiating to. Consider cell i, then we have

$$\begin{cases} L^i(a_j(t), e_j(t)) = L_0 + (L_M - L_0)a_j(t)\delta_{1,e_j(t)} + (L_A - L_0)a_j(t)\delta_{2,e_j(t)}, \\ W^i(a_j(t), e_j(t)) = W_0 + (W_M - W_0)a_j(t)\delta_{1,e_j(t)} + (W_A - W_0)a_j(t)\delta_{2,e_j(t)}, \end{cases} \tag{9.17}$$

where δ_{ij} denotes the Kronecker Delta. This function takes into account that different end shapes of adipocytes and myocytes. Note that $L_A = W_A$ to keep the end morphology of adipocytes circular. Further, $L_0 = W_0$ is the radius of the circular stem cells.

9.2.1.5 Mechanical Approach

For the computation of the octahedral shear strain, the mechanical balance is solved. To this extent, we use the Navier–Cauchy formulation to solve

$$\nabla \cdot \underline{\underline{\sigma}} + \mathbf{F}_M + \mathbf{F}_G = 0, \tag{9.18}$$

in Ω with a spring boundary condition

$$\underline{\underline{\sigma}} \cdot \mathbf{n} + K\mathbf{u} = 0, \tag{9.19}$$

on $\partial\Omega$. Here K represents a spring force on the boundary of the domain exerted by the surrounding tissue. Further, the oscillatory pulling (contraction) forces that are exerted by the myoblasts and myocytes are embedded within $\mathbf{F}_M$ and the forces exerted by the expanding adipocytes and myocytes are incorporated in the $\mathbf{F}_G$ term. For the two-dimensional setting where all cells are living *on* a substrate, this force does not exist and hence $\mathbf{F}_G = 0$. In a three-dimensional setting, the last-mentioned force should be incorporated. We also incorporate the expansion force in the 2D setting for the sake completeness of the algorithm. The myoblast force is decomposed into the separate contributions of all individual cells;

$$\mathbf{F}_M(t, \mathbf{x}, \overline{a}(t)) = \sum_{j=1}^{n_c(t)} \mathbf{F}_j^M(t, \mathbf{x}, a_j(t)), \tag{9.20}$$

where $\overline{a}(t) = \left[a_1(t), \ldots, a_{n_c(t)}(t)\right]^T$ represents the vector containing the maturation parameters of the viable cells. For the computation of the contraction force that is acted by cell j, we decompose surface of the cells into line segments of length $\Delta\Gamma$ with inward normal $\mathbf{n}$ (note that this vector is *outward* with respect to the domain of computation). Each of these line segment is treated as a point source exerting a force toward $\mathbf{n}$ directed *into* the cell. Therewith, at point $\mathbf{x}'$ on the cell boundary, the actual force becomes

$$\Delta\mathbf{F}_j^M(t, \mathbf{x}, a_j(t)) = P(t, a_j)\mathbf{n}\delta(\mathbf{x} - \mathbf{x}')\Delta\Gamma. \tag{9.21}$$

Subsequently, summing over all contributions on the boundary of cell j gives

$$\mathbf{F}_j^M(t, \mathbf{x}, a_j(t)) \approx \sum_{m=1}^{N} P(t, a_j)\mathbf{n}_m\delta(\mathbf{x} - \mathbf{x}_m)\Delta\Gamma, \tag{9.22}$$

where N represents the number of line segments on the cell boundary in the polygonal approximation of the cell. Further, $\mathbf{x}_m$ represents the midpoint of line segment m with unit normal vector $\mathbf{n}_m$ and length $\Delta\Gamma$. All these quantities correspond to cell j. Taking a limit $\Delta\Gamma \to 0^+$ (e.g., $N \to \infty$), gives

$$\mathbf{F}_j^M(t, \mathbf{x}, a_j(t)) = \int_{\partial\Omega_j} P(t, a_j)\mathbf{n}(\mathbf{x}\prime)\delta(\mathbf{x} - \mathbf{x}')d\Gamma', \tag{9.23}$$

where $d\Gamma'$ represents a line element and note that one has to integrate over $\mathbf{x}'$, which is in any case located on the cell boundary. Further, the quantity P should be considered as a force per unit length over the cell boundary. This force is used to quantify the force exerted by cell j on its extracellular tissue. An alternative formulation is to consider this force as a boundary condition on the region outside the cell. The boundary condition treatment will require adaptation of the computational grid at all times as the cell moves or expands. This grid adaptation will make the computations more expensive and, therefore, an alternative approach has been chosen in the present work. Because the diameters of the cells are much smaller than the domain of computation, and note that the boundary of the cell is divided into a sequence of point sources in the development of the chemical signal, we think that our treatment is reasonable and, as far as we know, the current treatment is original. We further note that the current treatment is applicable to any shape of cells. However, in the current study, we will barely use circular cross sections of the cells. The extension of the current formalism to three dimensions is straightforward as it is given by

$$\mathbf{F}_j^M(t, \mathbf{x}, a_j(t)) = \int_{\partial\Omega_j} P(t, a_j)\mathbf{n}(\mathbf{x}')\delta(\mathbf{x} - \mathbf{x}')dS', \tag{9.24}$$

where dS' represents a line element and note that one has to integrate over $\mathbf{x}'$, which is in any case located on the cell boundary. Furthermore, the quantity P should be considered as a force per unit area over the cell boundary in a three-dimensional case. In a fully analytic framework, one could use shifted radial Green's functions from elasticity for each cell to treat the cells really as point sources. This last-mentioned approach is omitted in the present study, but it will be applied in future analyses for the reason of its ease to use and its ultracheap computations. In the present work, we want to study the effects of the contraction and expansion of the tissue in relation with its surroundings as well. We model the activity of the subject by imposing a periodical time pattern on the forcing. For instance one can use

$$P(t, a, e) = \begin{cases} \widehat{P}(a)\cdot\cos(\omega t), & \text{if } e = 1, \\ 0, & \text{if } e = 2. \end{cases} \tag{9.25}$$

Here we use an increasing function for $\widehat{P}(a)$, as an example we take

$$\widehat{P}(a) = P_0 a. \tag{9.26}$$

Next we consider the pushing forces of the adipocytes and myocytes as a result of their growth. This issue is more important in 3D than 2D, nevertheless for the sake of generality we carry out the same discussion in 2D. We postulate that these forces are proportional to the time derivative of the cell area in 2D and to the time derivative of the cell volume in 3D. These forces are steady as long as the adipocytes do not change size. However, as they grow, the steady force that they exert on the extracellular tissue will change. We use a similar relation as earlier:

$$\mathbf{F}_j^G(t, \mathbf{x}, a_j(t)) = \int_{\partial\Omega_j} Q\mathbf{n}(\mathbf{x}')\delta(\mathbf{x} - \mathbf{x}')d\Gamma', \tag{9.27}$$

where Q represents the force per unit length exerted by the adipocytes on the extracellular structure, which only becomes active if the adipocyte is growing in area (in 2D) or in volume (in 3D)

$$Q = k\frac{dA}{dt} = \pi\left(L\frac{dW}{dt} + W\frac{dL}{dt}\right), \tag{9.28}$$

for the 2D case with an ellipse with axes L and W. Further, k is a nonnegative constant of proportionality. Note that this force is negative if the cell is shrinking.

9.2.1.6 Cell Migration

Mesenchymal stem cells are known to possess the property of *active* cell motility, whereas myocytes and adipocytes are immobile and only move if contact forces are applied to them or if they are subject to mechanical drag, also known as *passive migration*. In this work, we assume that *active* cell migration is determined by *chemotaxis* and random walk. Hence cell-based migration is modeled by

$$d\mathbf{x}_j(t) = \sigma d\mathbf{W}(t) + \mathbf{v}_p(t, \mathbf{x}_j(t))dt + 4\left(\mu_M a_j(1-a_j)\delta_{1,e_j(t)}\nabla c_M(t, \mathbf{x}_j(t)) + \mu_A a_j(1-a_j)\delta_{2,e_j(t)}\nabla c_A(t, \mathbf{x}_j(t))\right)dt. \tag{9.29}$$

The terms in the right-hand side determine the various migration modes. The first term denotes migration by random walk represents a measure of cell motility due to random walk. The σ parameter is related to cell diffusivity by $\sigma = \sqrt{2D}$, and $\mathbf{W}$ (t) is a vector Wiener process. The second term represents migration as a result of intercellular contact forces, see Vermolen and Gefen, and as a result of passive movement due to mechanical drag. The third term represents the contribution to migration as a result of chemotaxis where cells tend to migrate toward the gradient of a chemical. The term containing μ_M is active whenever $e_j(t) = 1$. It mimics the sensitivity of the cells with respect to the gradient of myocyte-secreted cytokines. The same, but now with respect to differentiation to the adipocyte phenotype, is exhibited in the μ_A-containing term.

9.3 NUMERICAL METHOD

We use a finite element method for the solution of the PDEs, such as the mechanical balance and all the chemical quantities. To obtain the mechanical signal on a cell, a postprocessing step of the finite element approximation is carried out. The Euler–Maruyama method is used to solve the stochastic differential equations. For completeness, we will describe the method in somewhat more detail.

9.3.1 The Finite Element Method for the Partial Differential Equations

We use the method that was proposed by Madzvamuse et al. (2003). The domain of computation is divided into a triangular mesh in 2D and into a tetrahedral mesh in 3D. Linear elements are used in all cases. The approach is based on the Galerkin finite element method where a weak form of the problem is constructed for all the PDEs. The solution, being the displacement or chemical quantities, is expressed as a linear combination of the unknowns at the mesh points. The development of the weak form is straightforward for the mechanical balance. For the chemical quantities, which we denote by c $(t, \mathbf{x})$ for reasons of illustration, we use the displacement of the mesh as a result of the mechanical forces that are exerted by the cells. Because the pulling and pushing forces by the cells imply the presence of a displacement field, which follows from the mechanical balance, the derivative of the displacement on each mesh point, which gives the mesh velocity, is computed by $\mathbf{v}(t, \mathbf{x}) = \frac{d}{dt}\mathbf{u}(t, \mathbf{x}(t))$, where u denotes the displacement on position $\mathbf{x}$ in the reference frame, and d/dt stands for the total time derivative (being the material derivative now). Then we have

$$\frac{\partial\phi}{\partial t} + \nabla\cdot\mathbf{J} = f(t, \mathbf{x}, \phi), \tag{9.30}$$

subject to initial and boundary conditions. Then to include the mesh velocity, the dynamics of the movement of the coordinates is incorporated in the above equation by the *passive* convection term $\nabla\cdot(\mathbf{v}\phi)$

$$\frac{\partial\phi}{\partial t} + \nabla\cdot(\mathbf{v}\phi) + \nabla\cdot\mathbf{J} = f(t, \mathbf{x}, \phi). \tag{9.31}$$

The product rule and the total derivative (material derivative) for ϕ gives

$$\frac{d\phi}{dt} + \phi(\nabla\cdot v) + \nabla\cdot\mathbf{J} = f(t, \mathbf{x}, \phi). \tag{9.32}$$

Using Galerkin's finite element method, we multiply the PDE by a test function $\varphi \in H^1(\Omega)$, which depends on time as a result of the temporal evolution of the mesh, for which Dziuk and Elliott (2013) proved

$$\frac{d}{dt}\varphi(t;\mathbf{x}(t)) = 0,$$

for Lagrangian basis functions, and we realize that

$$\frac{d}{dt}[\phi\varphi] = \frac{\partial}{\partial t}[\phi\varphi] + \nabla\cdot[\mathbf{v}\phi\varphi] - \phi\varphi(\nabla\cdot v).$$

Integration by parts and using the above equation gives

$$\int_{\Omega_t}\left(\frac{\partial(\phi\varphi)}{\partial t} + \nabla\cdot[\phi\varphi\mathbf{v}] + \varphi\nabla\cdot\mathbf{J}\right)d\Omega = \int_{\Omega_t}\varphi f d\Omega. \tag{9.33}$$

Subsequently, Gauss' theorem is applied on the second term and the third term is integrated by parts to get

$$\int_{\Omega_t}\left(\frac{\partial(\phi\varphi)}{\partial t} - \nabla\varphi\cdot\mathbf{J}\right)d\Omega + \int_{\partial\Omega_t}\varphi(J\cdot\mathbf{n} - \phi\mathbf{v}\cdot\mathbf{n})d\Gamma = \int_{\Omega_t}\varphi f d\Omega. \tag{9.34}$$

Finally we apply Reynold's transport theorem to get

$$\frac{d}{dt}\int_{\Omega_t}\phi\varphi d\Omega - \int_{\Omega_t}\nabla\varphi\cdot\mathbf{J}d\Omega + \int_{\partial\Omega_t}\varphi J\cdot\mathbf{n}d\Gamma = \int_{\Omega_t}\varphi f d\Omega. \tag{9.35}$$

The above boundary integral is further elaborated based on the boundary conditions. The numerical approximations are written in terms of linear combinations of basis functions with time-dependent weights. The backward Euler method is used to integrate the resulting system of ordinary differential equations over time. An IMEX method is used in the case of nonlinear equations.

9.3.2 The ZZ-Gradient Recovery Method

We need to determine the strain to get the octahedral shear strain as well as the strain energy density including its gradient. Furthermore, we need to determine the gradient of chemokines for the haptotaxis part of the cellular migration. This requires the determination of spatial derivatives of the displacement, which follows from the mechanical balance equation. Because we obtain the displacement field as a finite element approximation on the basis of piecewise linear basis functions, the error is of order $O(h^2)$, where h represents a measure for the elements. However, determining the gradient could lead to a decreased order, and furthermore, because we need to project the result on the positions (the centers) of the cells by the use of interpolation, the accuracy of the solution on the cellular positions could be further worsened. To prevent this to happen, we use the so-called ZZ-patch recovery method by Zienkiewicz and Zhu (1992a,b). For completeness we explain the main principles of the method. Suppose that we need to determine the derivative of a quantity u, say $\varepsilon = \frac{\partial u}{\partial x}$, then on each element the ε_h can be determined from the finite element solution. In this way, using linear elements, the variable ε_h is constant over each element. The idea is that we determine ε on the mesh points. Consider a mesh point, say $\mathbf{x}_k$, then we use a *patch* around $\mathbf{x}_k$, that consist of all the elements that contain mesh point $\mathbf{x}_k$ as a vertex. In each element of the patch, we determine ε_h. Then we want to determine a smoothed version of ε_h, which we call $\varepsilon^* = P\mathbf{a}$, then we determine ε^* such that

$$\text{Find } \varepsilon^* \text{ such that } \quad F(\varepsilon^*) \le F(\varepsilon), \quad \text{for all } \varepsilon, \quad \text{where } F(\varepsilon) = \sum_{j=1}^{N}\left(\varepsilon_h(\mathbf{x}_j) - \varepsilon_j^*\right)^2,$$

where $P = [1\ x\ y]$ for linear elements in 2D and N denotes the number of sampling points. In the case of linear elements, we use one sampling point per element; hence, in this case N is equal to the number of elements in the patch of mesh point $\mathbf{x}_k$. In the case of linear elements, one takes the midpoint of all elements that contain a certain shared vertex. In the above equation, one determines the vector $\mathbf{a}$. This least-squares problem gives the following system of linear equations for $\mathbf{a}$:

$$\sum_{j=1}^{N}P^T(\mathbf{x}_j)P(\mathbf{x}_j)\mathbf{a} = \sum_{j=1}^{N}P^T(\mathbf{x}_j)\varepsilon_h(\mathbf{x}_j)$$

The procedure is repeated for each vertex of the mesh and therewith a superconverging approximation for ε is obtained. This allows an accurate determination of the strain energy density as well of the octahedral shear strain. The procedure

along with its mathematical analysis are outlined in Zienkiewicz and Zhu (1992a,b). An alternative promising method could be the application of filtering techniques that were constructed and analyzed in Mirzaee et al. (2014).

9.3.3 Cell Maturation and Migration

First we update the cell maturation by use of the forward Euler's method, which reads as

$$a_j^{p+1} = a_j^p + \Delta t U\left(t^p, \tilde{\mathbf{x}}_j^p, \underline{\psi}(t^p), a_j^p\right), \tag{9.36}$$

for cell j, time t^p and on the p-th time step. From this equation, the differentiation axis is also determined. If a_j reaches one, then the new phenotype is adopted. The equations for the chemical concentrations are solved using an IMEX method where all nonlinear terms are evaluated at the previous time step, whereas the linear parts are incorporated at the new time step. The maturity of the cell and the differentiation axis are used from the new time step. To integrate the equations for cell migration over time, we divide the time into discrete time steps and use the Euler–Maruyama method to approximate the solution. Consider cell j, then

$$\begin{aligned}\tilde{\mathbf{x}}_j^{p+1} = \tilde{\mathbf{x}}_j^p + \mathbf{v}\left(t^p, \tilde{\mathbf{x}}_j^p\right)\Delta t + \sqrt{2D}\Delta\mathbf{W} + \left(\mathbf{u}\left(t^{p+1}, \tilde{\mathbf{x}}_j^f(t^{p+1})\right) - \mathbf{u}\left(t^p, \tilde{\mathbf{x}}_j^f\left(t^p\right)\right)\right) + \\ 4\left(\mu_M a_j^{p+1}\left(1 - a_j^{p+1}\right)\delta_{1,e_j(t^{p+1})}\nabla c_M\left(t^p, \tilde{\mathbf{x}}_j^p\right) + \mu_A a_j^{p+1}\left(1 - a_j^{p+1}\right)\delta_{2,e_j(t^{p+1})}\nabla c_A\left(t, \tilde{\mathbf{x}}_j^p\right)\right)\Delta t.\end{aligned} \tag{9.37}$$

where $\mathbf{v}$ denotes the velocity as a result of mechanical impingement determined by the gradient of the strain energy density. See Vermolen and Gefen (2012) for more details regarding this contribution. The gradient is determined by the use of the earlier ZZ-patch reconstruction method. Furthermore, the vectorial stochastic variable $\Delta\mathbf{W}$ (t^p) contains a vector with two or three realizations from a normal distribution as follows:

$$\Delta\mathbf{W} = [\Delta W_x \quad \Delta W_y \quad \Delta W_z]^T, \tag{9.38}$$

for the two-dimensional case, where ΔW_x, ΔW_y, and $\Delta W_z \sim \mathcal{N}(0, \Delta t)$ are three independent realizations from the normal distribution with zero mean and variance Δt. Furthermore, mechanical drag has been taken into account by the displacement vector over a time step Δt, see the third term between brackets in the above equation. Note that the displacements are obtained by mapping the solution of the displacement from mechanical equilibrium to the position of the centers of the cells. Because we use linear basis functions on the triangular finite element mesh, we use linear interpolation based on the finite element basis functions. The time stepping was chosen such that cells do not migrate more than one-fourth of their diameter. This warrants a sufficiently small time step such that numerical stability is obtained.

For clarity, we add a schematic of the algorithm that we used: Algorithm 9.1 Time-integration algorithm.

ALGORITHM 9.1 Time-Integration Algorithm

```
Initialise
n = 0; t = 0
while t < t_end do
    Compute Cellular Forces
    Compute Mechanical Displacements
    Update Mesh
    Compute Strain Energy Density
    Compute Concentration of Chemokines
    Map Solutions onto Cellular Positions
    Update Cell Maturations
    Update Cell Positions
    n ← n + 1
    t ← t + dt
end while
```

9.4 SIMULATIONS AND DISCUSSION

In this section, we show some examples of results that can be computed using the model. For all parametric choices, we refer to the thesis of Harrevelt (2015). The focus of the present chapter is on the numerical method, and thus the biological aspects are emphasized less. Because the strain is needed at the cellular positions, we use the ZZ-gradient recovery method that was described in the previous section. Fig. 9.3 shows the approximation of the gradient, using a direct gradient computation and using the ZZ-approach. It can be seen that the direct approach causes a discontinuous gradient pattern, which is not useful for the computation of the mechanical stimulus. The ZZ-recovery method gives a continuous gradient pattern as a result of the smoothening by incorporation of a patch of elements to approximate the gradient. Because the migrating cells may be located in several elements, this is an important improvement.

Subsequently, we show the results of two simulations in Fig. 9.4 to show what the model is capable of in terms of biological application. In the case of continuous exposure to cyclic mechanical force, the cells tend to differentiate to myocytes, whereas if cells are not exposed to any cyclic forces, then the stem cells tend to differentiate toward adipocytes. Although the parameters taken are mostly hypothetical, it can be seen that the model can be used to simulate both extreme cases. The input parameters have been given in Harrevelt (2015).

We note that the model qualitatively predicts well the concurrent differentiation to various phenotypes. The signals for differentiation are both chemical and mechanical, where in the latter case one has to use the gradient of a precomputed solution. Because the solutions of the mechanical force balance are continuous up to the second partial derivatives with respect to position, one should be able to use the derivatives of the solution. When computing the first-order derivatives of

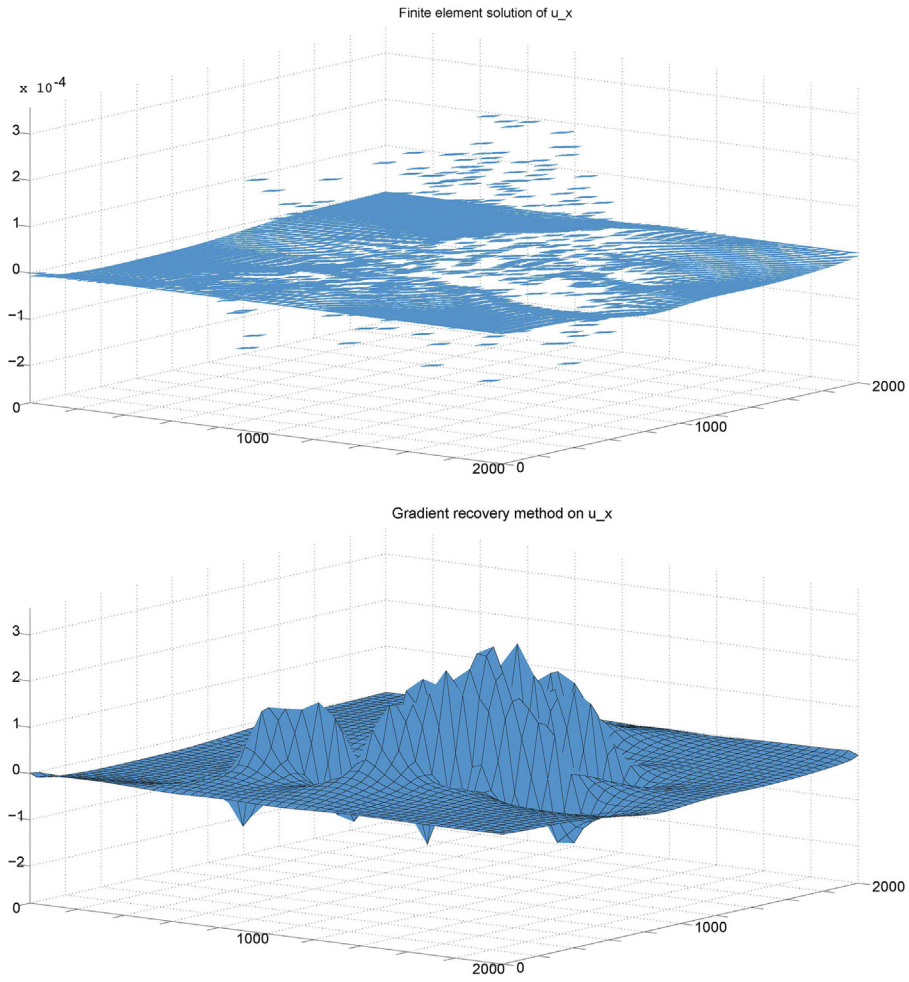

FIGURE 9.3 The approximation of the gradient of the solution (only $10^4 \frac{\partial u}{\partial x}$ is shown). Top: the direct method with discontinuities of the gradient over the element faces; bottom: the ZZ-approach with a continuous representation of the gradient.

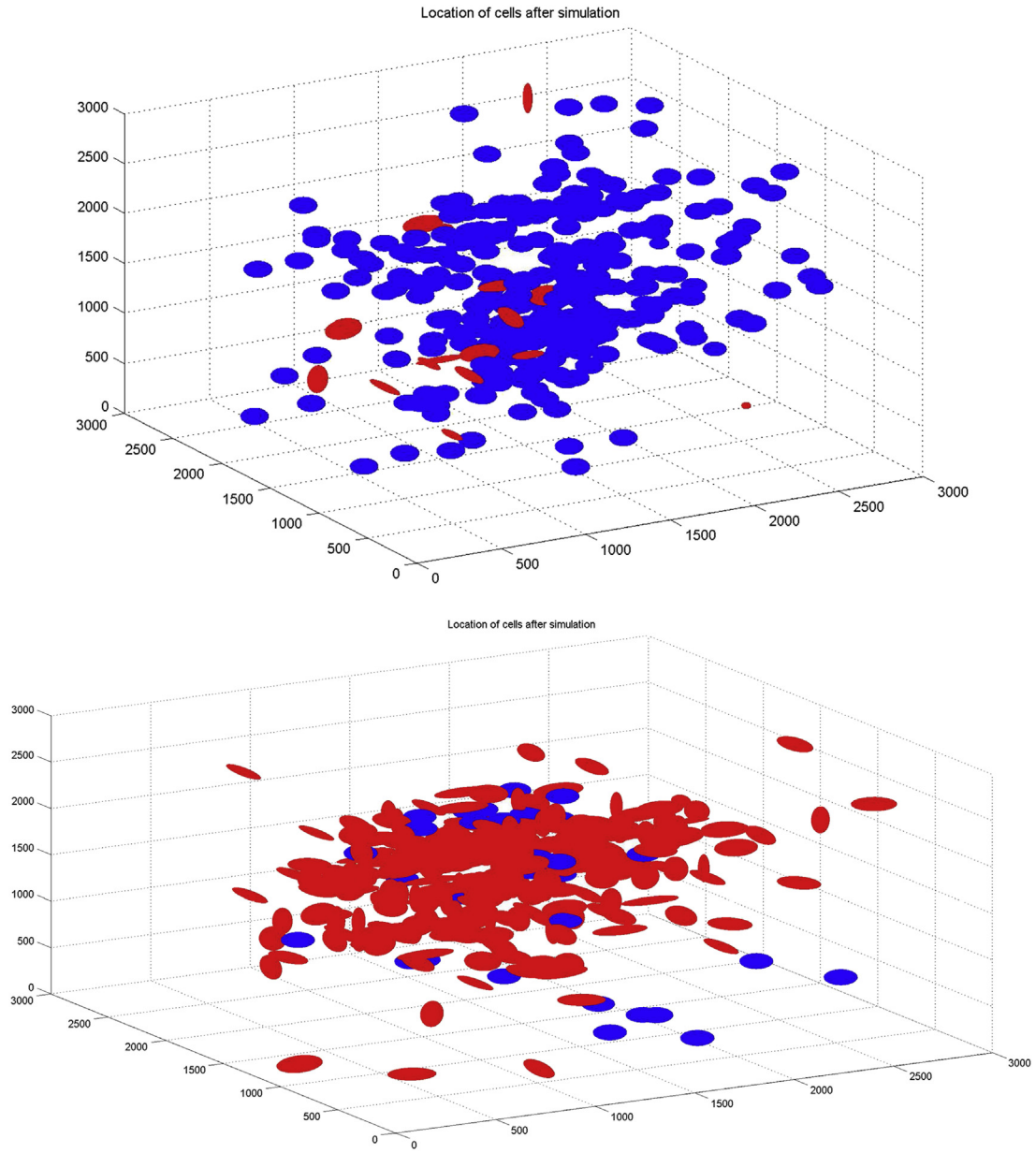

FIGURE 9.4 Myocytes and adipocytes after a period of exposure to noncyclic and cyclic loading on the top and bottom, respectively. The spherical blue (black in print versions) cells represent the (pre)adipocytes; the red (gray in print versions), more elongated, cells represent the muscle cells. Top: preferential differentiation to adipocytes; bottom: preferential differentiation to myocytes.

a finite element solution obtained with linear triangles, the gradient is discontinuous if a direct method is used, since over an element e with set of vertices $\mathbb{E}$, one obtains

$$\frac{\partial u}{\partial x} = \frac{\partial}{\partial x} \sum_{p \in \mathbb{E}} u_p \phi_p(x, y) = \sum_{p \in \mathbb{E}} u_p \frac{\partial \phi_p}{\partial x}, \tag{9.39}$$

where ϕ_p and u_p, respectively, represent the basis function of node p and (the approximation of) the solution on node p. This gives a discontinuity of the gradient over the element boundaries. An alternative is to use a weighed approach by considering the weak derivative. Then, one computes the gradient on the nodal points and one get a more smoothed representation of the solution. However, a disadvantage is that one still loses one order of accuracy, that is if the accuracy of the solution is $O(h^{p+1})$, then the accuracy possibly becomes $O(h^p)$. To prevent this loss of accuracy, one can use the

ZZ-patch gradient recovery method. In Zienkiewicz and Zhu (1992a,b), it is shown that the method does preserve accuracy. As an alternative, one can also use one of the filtering approaches that even increase accuracy, see Mirzaee et al. (2014) as an example. This is what we want to explore for this class of problems in the future. Both cell-based and continuum-scale models will likely benefit from this approach.

9.5 CONCLUSIONS

A numerical method for a cell-based model for cell migration and differentiation has been presented. The hybrid method resides on a combination of a moving mesh finite element method and a particle method and its interaction. The formalism can be used to model cell differentiation to various phenotypes at the same time. The signals can both be chemical and mechanical, where mechanical signals require the use of the gradient of the solution. The gradient of the solution is determined by the use of the ZZ-gradient recovery method. The method is generic and can be used for various applications involving cell differentiation. The currently presented formalism along with its numerical method can be generalized easily to applications with different cell phenotypes, if characteristics such as shape, strength, secretion rates, and migration speeds are known. For instance it is possible to treat fracture healing, which involves fibroblasts, osteoblasts, and chondrocytes analogously to what has been done in the present manuscript.

REFERENCES

Bookholt, F.D., Monsuur, H.N., Gibbs, S., Vermolen, F.J., 2016. Mathematical modelling of angiogenesis using continuous cell-based models. Biomechanics and Modelling in Mechanobiology 15 (6), 1577−1600.

Drasdo, D., Höhme, S., 2005. A single−cell−based model of tumor growth in vitro: monolayers and spheroids. Physical Biology 2 (3), 133−147.

Dziuk, G., Elliott, C.M., 2013. Finite element methods for surface PDEs. Acta Numerica 22, 289−296.

Gefen, A., Benayahu, D., 2015. The mechanobiology of obesity and related diseases. In: Studies in Mechanobiology, Tissue Engineering and Biomaterials, vol. 16. Springer−Verlag, Berlin Heidelberg.

Gimble, J.M., Katz, A.J., Bunnell, B.A., 2007. Adipose-derived stem cells for regenerative medicine. Circulation Research 100, 1249−1260.

Groh, A., Louis, A.K., 2010. Stochastic modeling of biased cell migration and collagen matrix modification. Journal of Mathematical Biology 61, 617−647.

Guilak, F., Cohen, D.M., Estes, B.T., Gimble, J.M., Liedtke, W., Chen, C.S., 2010. Control of stem cell fate by physical interactions with the extracellular matrix. Cell Stem Cell 5 (1), 17−26.

Harrevelt, S.D., 2015. Simulating the Differentiation of Stem Cells Using a 2D and 3D Mathematical Model (M.Sc.-thesis at the Delft Institute of Applied Mathematics). Delft University of Technology, The Netherlands. Downloadable at: http://repository.tudelft.nl.

Madzvamuse, A., Wathen, A., Maini, P.K., 2003. A moving grid finite element method applied to a biological pattern generator. Journal of Computational Physics 190, 478−500.

Mirzaee, H., Ryan, J.K., KIrby, R.M., 2014. Smoothness-increasing accuracy-conserving (SIAC) filters for discontinuous galerking solutions: application to structured tetrahedral meshes. Journal of Scientific Computing 58, 690−704.

Mousavi, S.J., Doweidar, M.H., Doblare, M., 2013. Modeling of cell migration: a mechano-chemo-electrotaxis approach. Journal of Theoretical Biology 329, 64−73.

Or-Tzadikario, S., Sopher, R., Gefen, A., 2010. Quantitative monitoring of lipid accumulation over time in cultured adipocytes as function of culture conditions: towards controlled adipose tissue engineering. Tissue Engineering (Part C) 16, 1167−1181.

Prokharau, P.A., Vermolen, F.J., Garcia−Aznar, J.M., 2012. Model for direct bone apposition on pre-existing surfaces, during peri-implant osseointegration. Journal of Theoretical Biology 304, 131−142.

Prokharau, P.A., Vermolen, F.J., Garcia−Aznar, J.M., 2014. A mathematical model for cell differentiation, as an evolutionary and regulated process. Computer Methods in Biomechanics and Biomedical Engineering 17 (10), 1051−1070.

Reinhart−King, C.A., Dembo, M., Hammer, D.A., 2008. Cell−cell mechanical communication through compliant substrates. Biophysics Journal 95, 6044−6051.

Rey, R., Garcia−Aznar, J.M., 2013. A phenomenological approach to modelling collective cell movement in 2D. Biomechanics and Modelling in Mechanobiology 12 (6), 1089−1100.

Sell, S., 2004. Stem cell origin of cancer and differentiation therapy. Critical Reviews in Oncology/Hematology 51 (1), 1−28.

Shoham, N., Girshovitz, P., Katzengold, R., Shaked, N.T., Benayahu, D., Gefen, A., 2014. Adipocyte stiffness increases with accumulation of lipid droplets. Biophysics Journal 106 (6), 1421−1431.

Stolzing, A., Jones, E., McGonagle, D., Scutt, A., 2007. Age-related changes in human bone marrow-derived mesenchymal stem cells: consequences for cell therapies. Mechanisms of Aging and Development 129 (3), 163−173.

Van Oers, R.F.M., Rens, E.G., LaValley, D.J., Reinhart−King, C.A., Merks, R.M.H., 2014. Mechanical cell−matrix feedback explains pairwise and collective endothelial cell behavior in vitro. PLoS Computational Biology 10 (3), e1003774.

Vermolen, F.J., Gefen, A., 2012. A semi-stochastic cell-based formalism to model the dynamics of migration of cells in colonies. Biomechanics and Modeling in Mechanobiology 11 (1−2), 183−195.

Vermolen, F.J., 2015. Particle methods to solve modelling problems in wound healing and tumor growth. Computational Particle Mechanics 2 (4), 381–399.

Vermolen, F.J., Gefen, A., 2015. Semi-stochastic cell-level computational modelling of cellular forces: application to contractures in burns. Biomechanics and Modeling in Mechanobiology 14 (6), 1181–1195.

Vermolen, F.J., Van der Meijden, R.P., Van Es, M., Gefen, A., Weihs, D., 2015. Towards a mathematical formalism for semi–stochastic cell–level computational modelling of tumor initiation. Annals of Biomedicine 43 (7), 1680–1694.

Weihs, D., Gefen, A., Vermolen, F.J., 2016. Review on experiment-based two- and three dimensional models for wound healing. Interface Focus 6, 20160038.

Wu, Y., Chen, L., Scott, P.G., Tredget, E.E., 2007. Mesenchymal stem cells enhance wound healing through differentiation and angiogenesis. Stem Cells 25, 2648–2659.

Yan, M., Liu, Q., 2016. Differentiation therapy: a promising strategy for cancer treatment. Chinese Journal of Cancer 35 (1), 3.

Zienkiewicz, O.C., Zhu, J.Z., 1992a. The superconvergent patch recovery and a posteriori error estimates. Part 1: the recovery technique. International Journal for Numerical Methods in Engineering 33 (7), 1331–1364.

Zienkiewicz, O.C., Zhu, J.Z., 1992b. The superconvergent patch recovery and a posteriori error estimates. Part 2: error estimates and adaptivity. International Journal for Numerical Methods in Engineering 33 (7), 1365–1382.

FURTHER READING

Byrne, H.M., Drasdo, D., 2009. Individual–based and continuum models of growing cell populations: a comparison. Journal of Mathematical Biology 58, 657–687.

Levy, A., Enzer, S., Shoham, N., Zaretsky, U., Gefen, A., 2012. Large, but not small sustained tensile strains stimulate adipogenesis in culture. Annals of Biomedical Engineering 40, 1052–1060.

Shoham, N., Gottlieb, R., Shaharabani-Yosef, O., Zaretsky, U., Benayahy, D., Gefen, A., 2012. Static mechanical stretching accelerates lipid production by adipocytes by activating the MEK signaling pathway. American Journal of Physiology and Cell Physiology 302, C429–C441.